Journal of Power Sources 240 (2013) 219–231

Contents lists available at SciVerse ScienceDirect

Journal of Power Sources

journal homepage: www.elsevier.com/locate/jpowsour

Electrocogeneration of hydrogen peroxide: Confocal and potentiostatic investigations of hydrogen peroxide formation in a direct methanol fuel cell

Korakot Sombatmankhong [a,*], Kamran Yunus [b], Adrian C. Fisher [b]

[a] National Metal and Materials Technology Center (MTEC), 114 Thailand Science Park, Paholyothin Rd., Klong 1, Klong Luang, Pathumthani 12120, Thailand
[b] Department of Chemical Engineering and Biotechnology, University of Cambridge, New Museums Site, Pembroke Street, Cambridge CB2 3RA, UK

HIGHLIGHTS

- Production, accumulation and removal of H_2O_2 were visualised at microscopic level.
- 3D distribution and concentration of H_2O_2 was quantified by fluorescence mapping.
- Effect of cell potential on cogeneration was studied by real-time investigations.
- Higher amount of H_2O_2 accumulation resulted in a decrease in cell potential.
- Electrocogeneration processes greatly improved with decreasing cell potentials.

ARTICLE INFO

Article history:
Received 11 January 2013
Received in revised form
2 March 2013
Accepted 6 March 2013
Available online 12 April 2013

Keywords:
Direct methanol fuel cell
Confocal laser scanning microscopy
Microfabrication
Electrocogeneration
Hydrogen peroxide

ABSTRACT

This work aims to fulfil some of the critical challenges associated with the electrochemical processes in commercialisation of an electrocogeneration direct methanol fuel cell: the understanding of the formation, decomposition and removal of hydrogen peroxide at the cathodic chamber. The better understanding of operating conditions on improving the electrocogeneration performance is also valuable for developing an optimal operating condition that enhances electrocogeneration activity. The production and removal of hydrogen peroxide are investigated by sensing the fluorescence signal in the cathodic chamber using confocal microscopy. It is found that the higher production of hydrogen peroxide promotes the intensity but reduces the cell potential due to the depletion of fresh reactant and the accumulation of hydrogen peroxide. Consequently, hydrogen peroxide should be removed efficiently in order to maintain the cell performance. The three-dimensional distribution and concentration of hydrogen peroxide are quantified at various operating potentials using fluorescence mapping, which is a correlation between the fluorescence signal and the concentration of hydrogen peroxide. The simultaneous fluorescence and potentiostatic investigations indicate that the electrocogeneration process is improved significantly by decreasing the cell potentials; the current efficiencies of 85.00, 64.78 and 51.13% are obtained at the operating potentials of 300, 400 and 550 mV respectively.

1. Introduction

An electrocogeneration fuel cell is a power generator and a chemical reactor that directly converts chemical energy into electricity plus useful chemicals. This novel type of fuel cells has become a promising alternative to a conventional chemical reactor and a traditional fuel cell that produces water as a by-product [1]. In general, an electrocogeneration process involves electrochemical reactions occurring in a conventional fuel cell; when the fuel and oxidant are supplied individually to the cell, electrons are harnessed through an external load while useful products are collected by a chemical recovery system.

Several electrocogeneration fuel cells were primarily developed in the middle of the 20th century in order to shorten a complicated chemical process to a single-step production [2]. The key benefits of electrocogeneration fuel cells over the conventional catalytic processes include:

(i) The reactants are supplied separately to the system; consequently they do not compete at the same reaction sites and the explosion risk is reduced.

* Corresponding author. Tel.: +66 2564 6500x4706; fax: +66 2564 6403.
E-mail address: Korakots@mtec.or.th (K. Sombatmankhong).

0378-7753/$ – see front matter © 2013 Elsevier B.V. All rights reserved.
http://dx.doi.org/10.1016/j.jpowsour.2013.03.183

(ii) The reactor can be reduced in size with minimal corrosion. The required operating temperature is much lower.
(iii) The chemical production and selectivity of the process can be altered by varying either the external load or the electrode potential. The electrode catalyst also plays an important role in altering the selectivity.
(iv) The use of reactants is economical since they can be recirculated.

Most of the chemicals produced from the electrocogeneration processes have been commercially attractive such as cyclohexylamine [3], 1-propanol [4] and hydrogen peroxide [5–7]. Among these chemicals, hydrogen peroxide has received an increasing interest in a wide range of industrial processes such as the bleaching of mechanical pulp and the brightening of chemical pulp in the paper industry. Apart from the bleaching operational processes, the electrocogeneration fuel cells are particularly useful for remote applications, local waste water treatment and oxidation of organic compounds. Hydrogen peroxide has been used to replace other chemical oxidants due to low environmental impact. For example, chlorine is also used as a bleaching agent for wood-pulp industries but generates toxic chlorinated products. On the other hand, hydrogen peroxide undergoes oxidation of organics and then transforms into non-contaminant products including water and oxygen. Since 1957, the majority of hydrogen peroxide has been manufactured by the anthraquinone process [8] which is a catalysis process comprised of a multi-step operation that consumes high energy; hence, the production of hydrogen peroxide through this process is costly. In addition to the production cost, decomposition of hydrogen peroxide is thermodynamically favourable ($\Delta G^{\circ} = -119.2$ kJ mol^{-1}) and the rate of decomposition depends on the temperature, the concentration of hydrogen peroxide and the presence of impurities and stabilisers. Consequently, a simple reactor should be installed on site to produce hydrogen peroxide in the end-use industries which then reduces the production cost and improves the utilisation of hydrogen peroxide.

Electrocogeneration fuel cells meet all the requirements with an additional benefit of power generation. In the early stages of the development, Oloman and Watkinson [9] developed a trickle bed electrochemical reactor to produce alkaline peroxide solutions by the reduction of oxygen. The reactor was composed of a packed bed cathode made of graphite particles which was separated from a metal anode plate by a porous diaphragm. Oxygen and sodium hydroxide were fed concurrently through the cell while a current density of 100 mA cm^{-2} was supplied across the anode and cathode at 60 °C, leading to a production of 2 wt.% hydroperoxide ion in 6 wt.% sodium hydroxide with the current efficiency of 75%. Later on, economical reactors that do not require the passage of current to drive the electrochemical reactions have been proposed. Otsuka and Yamanaka [10] have proposed a hydrogen/Nafion® 117/oxygen fuel cell to cogenerate hydrogen peroxide and electricity using different catalyst materials on the cathode such as platinum, palladium, gold and graphite. By using platinum catalyst, the current efficiency for the formation of hydrogen peroxide was initially 100% with the maximum concentration of 0.2 wt.% (i.e. ~59 mM) and the current density of 30 mA cm^{-2}. After a period of time, the efficiency decreased dramatically since hydrogen peroxide was further electrochemically reduced at the active platinum and/or thermally decomposed by the waste heat released from the fuel cell reaction. Less active catalysts such as graphite or gold mesh was found to have better long-term current efficiency. A similar work was carried out in a new reactor design using a porous cathode made of hot-pressed carbon and PTFE powder [7]. The porous graphite structure allowed effective access of oxygen to the active sites; hence, the production of hydrogen peroxide was improved. Sodium hydroxide solution was continuously supplied to the cathodic chamber as an additional catholyte to provide an alkaline environment and to remove hydrogen peroxide from the cell. The discharged solutions contained hydrogen peroxide up to 7 wt.% (2.06 M) with the maximum current density of 100 mA cm^{-2}. Instead of Nafion® 117, potassium hydroxide was used as an alternative in an undivided fuel cell. With the simpler design, however, a smaller amount of hydrogen peroxide (<22.5 mM) was obtained [6].

Agladze and co-workers [11] developed a direct methanol fuel cell (DMFC) that is composed of the Nafion 115 membrane sandwiched by the "Black Pearls 2000" cathode and the carbonaceous anode (Pt). A mixture of 1 M methanol and 7 M potassium hydroxide was supplied to the anode while air was fed to the cathode with the additional feed of sodium chloride brine or seawater catholyte. The current efficiency of 87–95% and the current density of 15 mA cm^{-2} were generated at the production rate of 5.286–9.44 mg h^{-1} cm^{-2}.

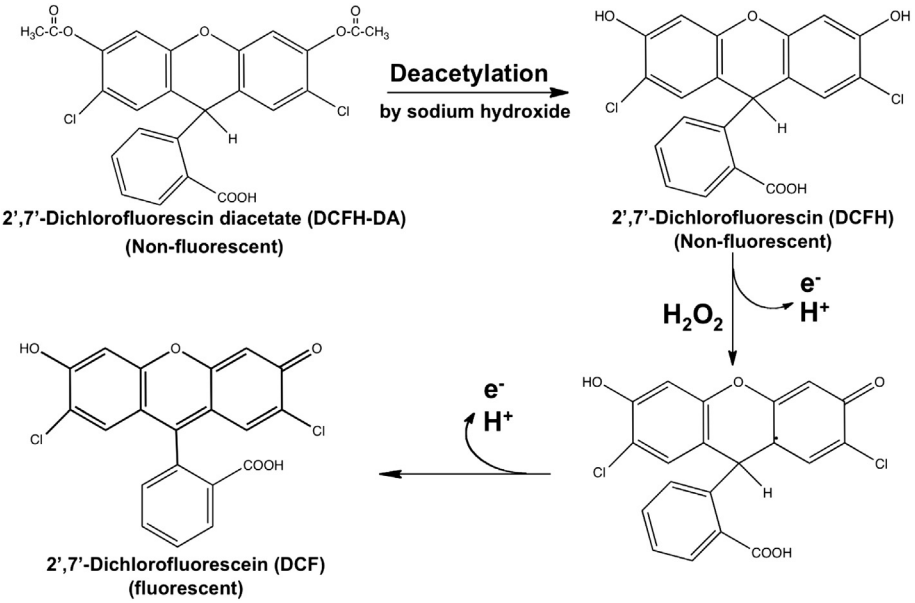

Fig. 1. Reaction mechanism of dichlorofluorescin synthesis and oxidation. The non-fluorescent DCFH is rapidly oxidised to highly fluorescent DCF with the presence of hydrogen peroxide.

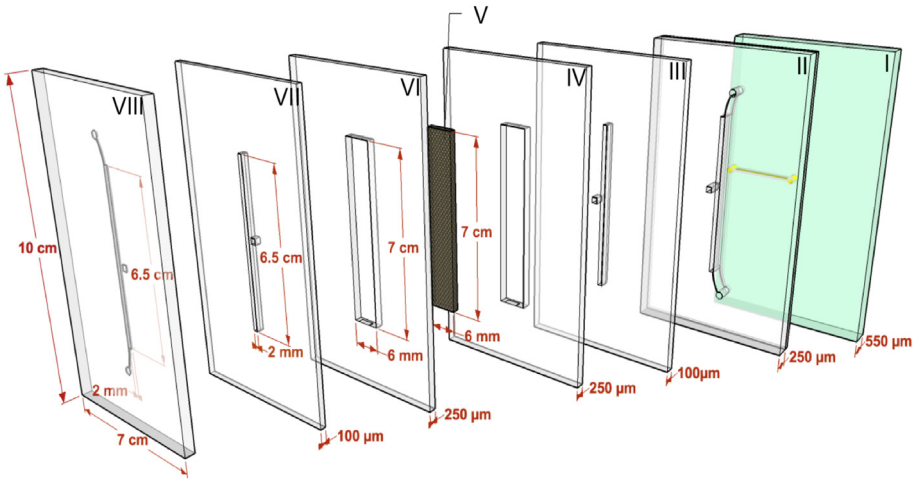

Fig. 2. Schematic diagram of the transparent compositions fabricated by photolithography to allow optical access to the electrocogeneration MEA (layer V).

The electrocogeneration process of a DMFC to cogenerate hydrogen peroxide and electricity has not been studied extensively. There are several challenges associated with the electrocogeneration technology including: (i) the development of economical catalyst materials with an improved durability and selectivity, (ii) the understanding of electrocogeneration reactions (i.e. entropy and hot spots), (iii) the formation, decomposition and removal of hydrogen peroxide at the cathodic chamber and (iv) the better understanding of operating conditions on improving the electrocogeneration performance. Therefore, the present work aims to fulfil some of the critical challenges associated with the electrocogeneration DMFC. *In situ* formation, accumulation and removal of hydrogen peroxide produced at the cathodic chamber were investigated at microscopic level for the first time using confocal laser

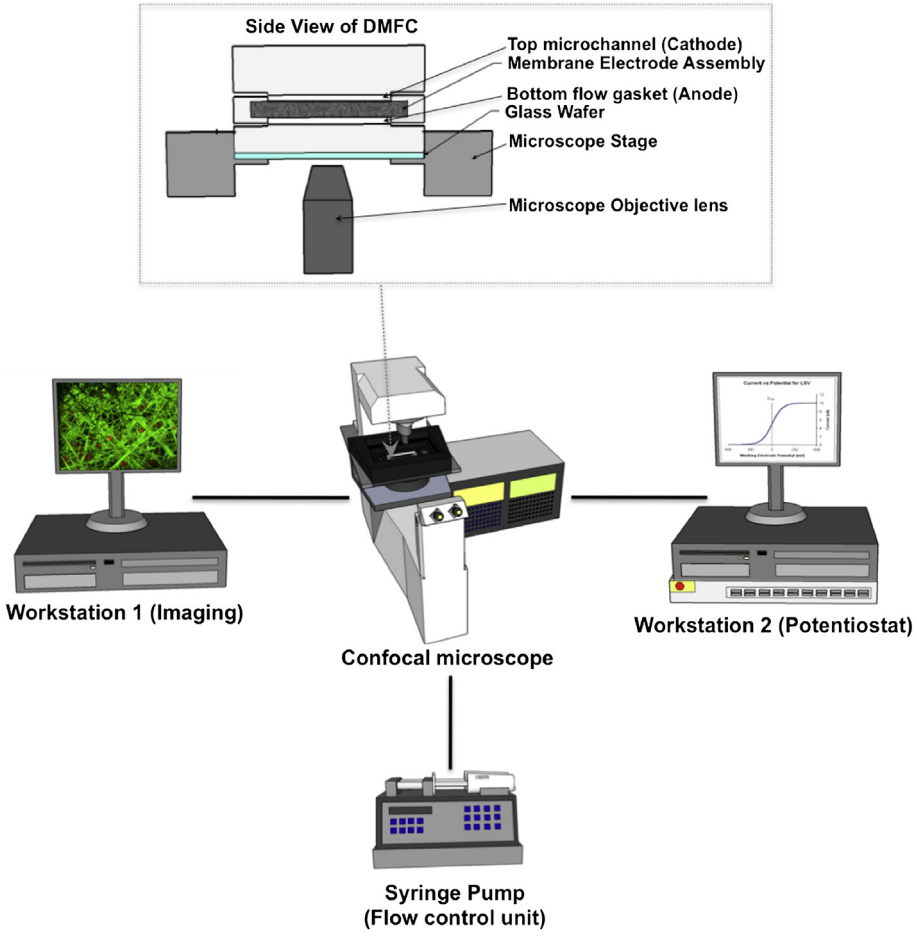

Fig. 3. The experimental set-up for the simultaneous investigations.

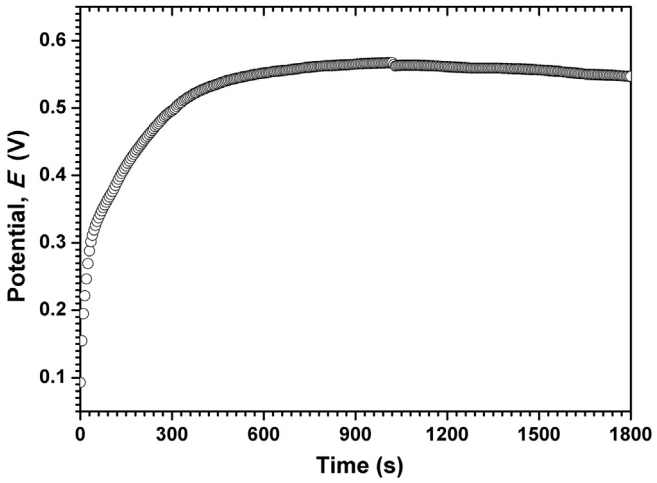

Fig. 4. Open circuit potential of DMFC with electrocogeneration system recorded during the conditioning process.

scanning microscopy. Dichlorofluorescin (DCFH), a highly sensitive fluorescent probe, was employed to trace the presence of as low as 25 pmol peroxide [12]. Quantification of hydrogen peroxide production was also characterised by fluorescence mapping. Moreover, the effect of operating potential on current efficiency and electrocogeneration performance was determined by simultaneous visualisation and current investigations. These fundamental studies will be valuable for developing an optimal condition that enhances electrocogeneration activity. As a result, the practical use of the electrocogeneration DMFC will be applicable and affordable for real applications.

2. Materials and methods

The electric current and hydrogen peroxide (or hydroperoxide ion (HO_2^-)) can be generated simultaneously from two electrocatalytic reactions using methanol as a fuel and oxygen as an oxidant. The half–cell reactions of the electrocogeneration process [2] are given below:

Anode

$$CH_3OH + H_2O \rightarrow CO_2 + 6H^+ + 6e^- \quad E_a^o = -0.081\ V \tag{1}$$

Cathode

$$O_2 + 2H^+ + 2e^- \rightarrow H_2O_2 \quad E_c^o = +0.690\ V \tag{2}$$

Overall reaction (via two-electron transfer reduction of oxygen)

$$CH_3OH + 3O_2 + H_2O \rightarrow CO_2 + 3H_2O_2 \quad E^o = 0.609\ V \tag{3}$$

Unfavourable half–cell reactions may occur depending on the catalyst selectivity and the operating potential [2]. This involves the cathodic reaction occurring in a conventional DMFC. Unlike the electrocogeneration process, oxygen undergoes four-electron reduction to produce water at the cathode:

$$O_2 + 4H^+ + 4e^- \rightarrow 2H_2O \quad E_c^o = 1.21\ V \tag{4}$$

Overall reaction (via four-electron transfer reduction of oxygen)

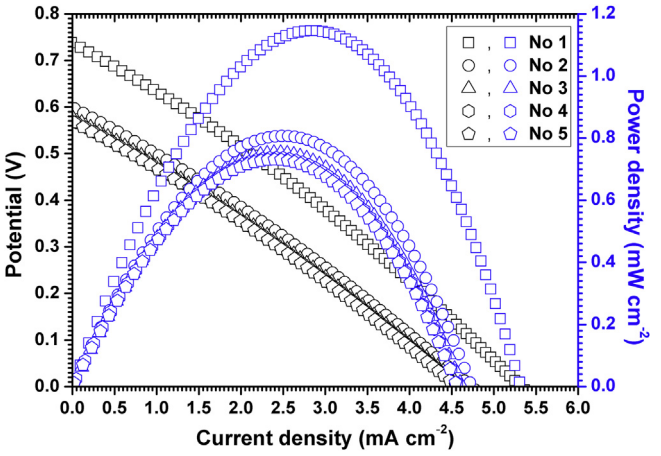

Fig. 5. Polarisation and power curves recorded after the conditioning process. The linear voltammetry performed five times (from scan number 1–5) repetitively, at a fixed potential scan rate of 100 mV s^{-1}.

$$2CH_3OH + 3O_2 \rightarrow 2CO_2 + 4H_2O \quad E^o = 1.129\ V \tag{5}$$

Although the theoretical open circuit potential of the electrocogeneration DMFC is much lower than that of the conventional one, the benefits of the electrocogeneration process that simultaneously generates electricity and hydrogen peroxide at low cost are the most significant.

2.1. Materials

All experiments were carried out with a membrane electrode assembly (MEA) sandwiched between two gas diffusion layers (GDLs). Nafion® 117 was used as a polymer electrolyte membrane (PEM). The catalysts loaded on the anode and cathode were platinum (1.256 mg cm^{-2}) and pure cobalt powder (0.5 mg cm^{-2}) respectively. The electrode materials were generously supplied by Johnson Matthey.

All chemicals were purchased from Sigma Aldrich®. All solutions were freshly prepared and used immediately for every measurement.

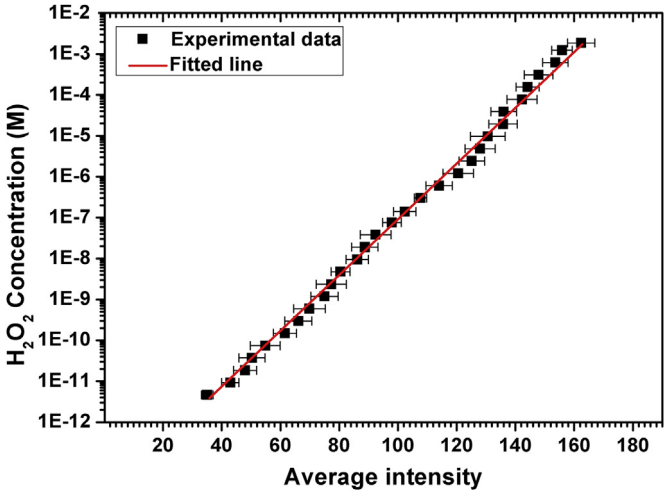

Fig. 6. A semi-log scale plot of average fluorescent intensity versus hydrogen peroxide concentration. The fluorescence intensities of the standard DCFH solutions containing different concentrations of hydrogen peroxide from 4.634 pM to 1.866 mM were investigated by a Leica TCS SPE microscope.

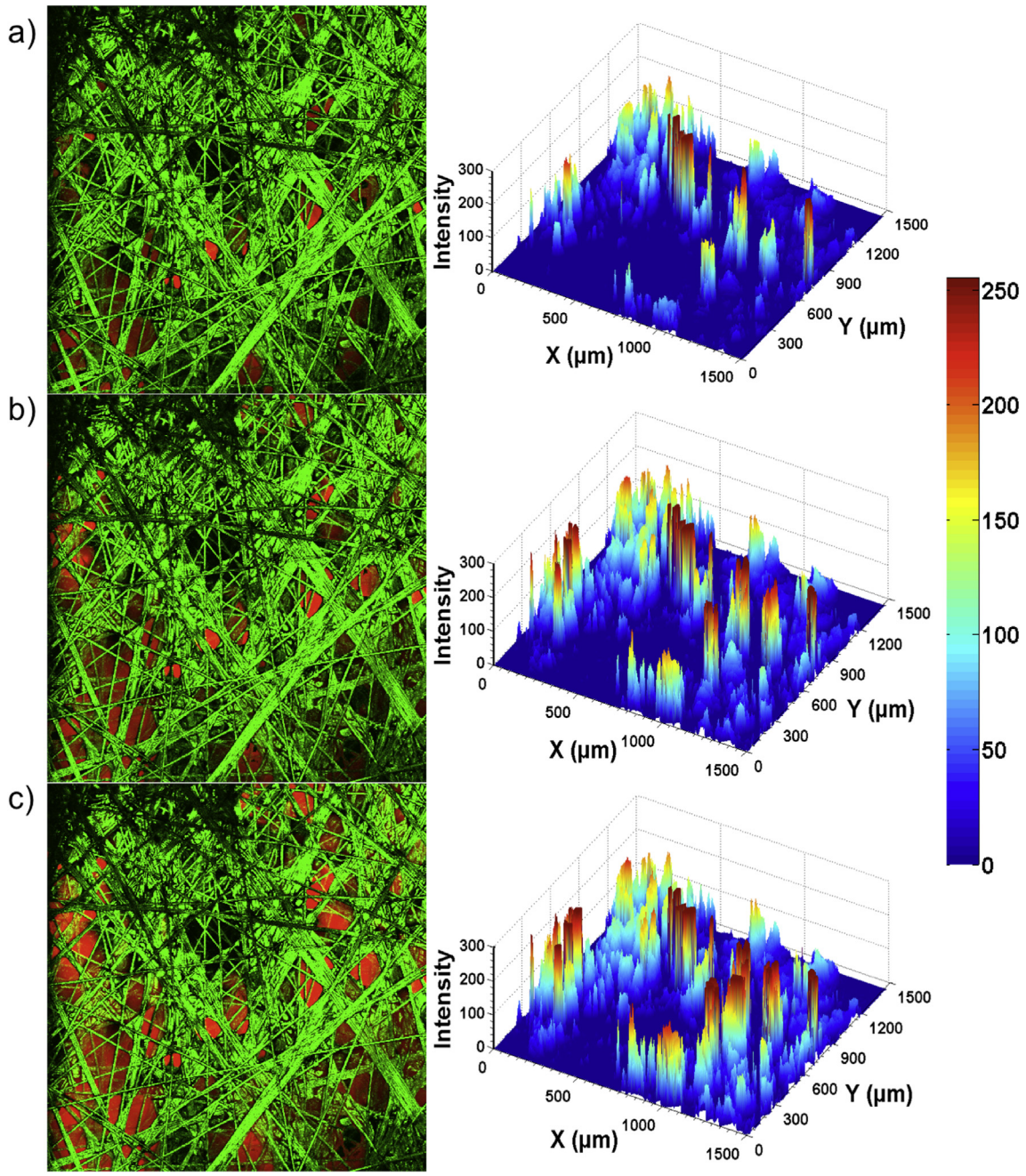

Fig. 7. Real-time visualisation of hydrogen peroxide formation in a DMFC with electrocogeneration system. The time-series confocal images and corresponding three-dimensional intensity plots are shown in chronological order as follows: (a) 0.02, (b) 2.21 and (c) 10.98 min. All images are displayed at the same focal plane of 50 μm inside the GDL. The green and red colours represent the reflection of the carbon spindles and a fluorescent signal, respectively. Continuation of the real-time visualisation of hydrogen peroxide formation in a DMFC with electrocogeneration system. The time-series confocal images and corresponding three-dimensional intensity plots are shown in chronological order as follows: (d) 28.51, (e) 82.21 and (f) 101.67 min. All images are displayed at the same focal plane of 50 μm inside the GDL. The green and red colours represent the reflection of the carbon spindles and a fluorescent signal, respectively. (For interpretation of the references to colour in this figure legend, the reader is referred to the web version of this article.)

2.2. Preparation of dichlorofluorescin dye solution

2′,7′-Dichlorofluorescin (DCFH) was prepared from 2′,7′-dichlorofluorescin diacetate (DCFH-DA), based on the method developed by Cathcart and co-workers [12]. On the other hand, the method was slightly modified to provide a suitable concentration and oxidant solution. The reaction mechanism of the DCFH synthesis is illustrated in Fig. 1. 0.2 ml of 30 mM DCFH-DA in dimethyl sulfoxide (DMSO) was added to 24 μl of 10 N sodium hydroxide to convert DCFH-DA to DCFH. Then, the reaction mixture was stirred at room temperature for 30 min to ensure the completion of the deacetylation reaction. After that, the mixture was neutralised with 600 μl of 5 M sodium phosphate buffer (pH 7.4), followed by adding 50 ml of distilled water. The final DCFH concentration is 116.8 M containing dissolved oxygen at ambient temperature (i.e. ∼260 μM at 25 °C [13]) which was subsequently employed as an oxidant in the electrocogeneration DMFC.

It was noted that the DCFH solution must be stored on ice in the dark until used and then discarded each day after use.

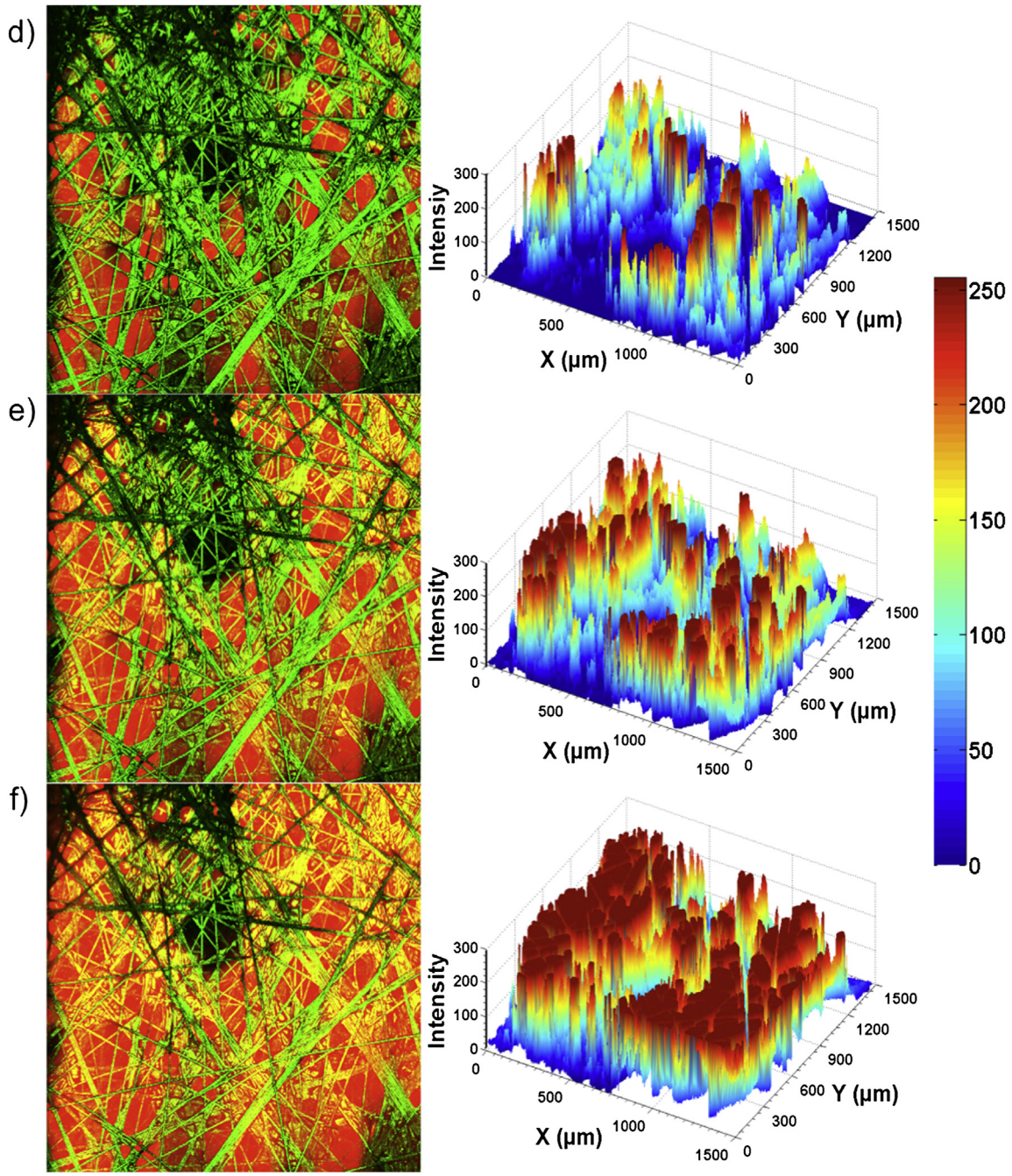

Fig. 7. (*continued*).

2.3. Solution calibration for fluorescence mapping

The quantitative analysis of hydrogen peroxide generation was carried out using fluorescence mapping: a relationship between hydrogen peroxide concentration and fluorescence intensity. To prepare standard DCFH solutions, 116.8 μM of DCFH solution was initially prepared in separate bottles. Then, different amounts of hydrogen peroxide were added into the bottles to provide the standard DCFH solutions containing different concentrations of hydrogen peroxide (4.654 pM–1.866 mM). After that, the fluorescence intensity of the standard solutions was examined by a Leica TCS SPE microscope. It is noted that the investigation was carried out using an identical experimental setup as used for the electrocogeneration DMFC. The fluorescence data was obtained from three independent experiments and are expressed as mean ± standard deviation.

2.4. Fabrication of a transparent DMFC device for study of electrocogeneration process

The scanning size of confocal microscopy is limited by the opacity of MEA. For this reason, a miniaturised fuel cell is a good alternative solution for this application. A transparent device was fabricated by soft lithography and the cell configuration is shown in Fig. 2. The device was composed of seven composite layers:

(i) Layer I: A 0.55 mm thin glass wafer having a gold microelectrode as an electrical connection on the cathode side of MEA,
(ii) Layer II, IV and VI: 250 μm-thick polydimethylsiloxane (PDMS) gaskets that were cast from SU-8 moulds, fabricated by a standard soft lithography,
(iii) Layer III and VII: 100 μm-thick PDMS gaskets,
(iv) Layer V: A MEA for a methanol/oxygen electrocogeneration system, having its cathode facing toward the glass wafer (Layer I), and
(v) Layer VIII: a PDMS microchannel fabricated by soft lithography using an identical SU-8 mould for casting Layer II.

The layer-by-layer assembly was carried out using plasma treatment. The active surface area of the electrode was 1.3 cm^2.

2.5. Testing procedure

The experimental setup for simultaneous visualisation and current investigations is demonstrated in Fig. 3. Confocal laser scanning microscope was used to investigate the production of hydrogen peroxide at the cathodic chamber during cell operation. According to the dye chemistry in Fig. 1, the fluorescence detection indicates the formation of hydrogen peroxide from the electrocogeneration process. Two excitation wavelengths of 458 nm and 496 nm were employed at the same time to detect the fibrous structure of the GDL and the fluorescence intensity respectively. The time-series confocal images were taken at the same horizontal plane (XY plane) with a minimum time step of 1.315 s. Overlays of the two spectral channels enabled the view of carbon fibres and hydrogen peroxide in the same images. To construct a three-dimensional distribution of hydrogen peroxide in the cathodic chamber, single XY images were taken across the *Z*-axis at an interval of 1 μm. All the images were processed by Matlab.

Prior to visualisation, the electrocogeneration fuel cell was conditioned by passing the DCFH solution and 2 M methanol solution to cathode and anode respectively. The conditioning process was performed for 30 min along with the chronopotentiometric measurement at zero current. After that, linear voltammetry was performed repetitively to draw the polarisation curves from the cell until the cell performance was stable. Next, simultaneous visualisation and chronoamperometry was undertaken to evaluate the current efficiency of the electrocogeneration fuel cell under different operating potentials. It is noted that the co-flow configuration was employed in all experiments.

To explore the influence of the operating potential, chronoamperometry was used to control the cell potentials and record the current responses throughout the investigations. Three negative potentials of 200, 100 and 5 mV were applied to the system resulting in an overall cell potential of 300, 400 and 550 mV, respectively.

3. Results and discussions

3.1. Characteristics of polarisation and open circuit potential in a DMFC electrocogeneration system

A conditioning process of the electrocogeneration DMFC was conducted in order to achieve a stable cell performance prior to the simultaneous investigations. The open circuit potential of the electrocogeneration process recorded during the conditioning process is shown in Fig. 4. It is found that the cell potential reaches its plateau ($E \sim 0.57$ V) after 500 s; however, the open circuit potential is relatively lower than the thermodynamic potential ($E = 0.609$ V in Equation (3)). This is attributed to the methanol crossover often associated with the DMFC [14].

The five consecutive scans of polarisation and power curves (shown in Fig. 5) were obtained using linear voltammetry, at a fixed potential scan rate of 100 mV s^{-1}. The decrease in peak power with scan numbers is caused by the accumulation of hydrogen peroxide and carbon dioxide by-products at the active sites; this reduces the active surface area for the reactions to occur. The power peaks obtained at scan number 4 and 5 are relatively unchanged indicating the completion of the conditioning process. The electrocogeneration DMFC exhibits a current density of 4.5–5.3 mA cm^{-2} and power density of 0.8–1.2 mW cm^{-2}, which is still very low and should thus be stacked with one another in order to produce a useful amount of power for portable applications (in the range of 0.5–20 W [15]). The low performance of the electrocogeneration process is owing to the limitation of oxygen solubility in the DCFH solution (i.e. ~260 μM at 25 °C [13]), used as the oxidant media. This level of dissolved oxygen, however, yields a sufficient amount of hydrogen peroxide to be detected by DCFH dye. More details and discussions are given in the following section.

3.2. Fluorescence mapping: a relationship between fluorescence signal and hydrogen peroxide concentration

With the use of an identical experimental setup and optical configuration in all experiments, a relationship between the fluorescence intensity and the hydrogen peroxide concentration can be obtained and then used to determine the quantity of hydrogen peroxide production under real fuel-cell operating conditions. Fig. 6 shows the semi-log scale plot of the average fluorescence intensity versus the hydrogen peroxide concentration. The efficiency of DCFH oxidation is dependent on the concentration of hydrogen peroxide [12] as the fluorescence intensity is found to increase with the quantity of hydrogen peroxide existing in the standard dye solutions. The sensitivity of non-fluorescent DCFH to the level of hydrogen peroxide could be achieved as low as 4.634 pM.

The red line indicates a linear regression fit between average intensity and hydrogen peroxide concentration. The fitted equation is expressed as:

$$[H_2O_2]_{avg} = \left(6.6071152231 \times 10^{-15}\right)\exp^{0.1625F} \quad (6)$$

where $[H_2O_2]_{avg}$ is an average concentration of hydrogen peroxide production and F is an average fluorescence intensity investigated

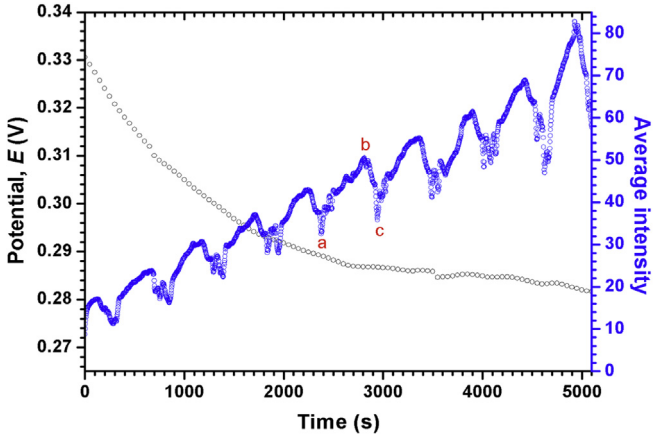

Fig. 8. Simultaneous visualisation of hydrogen peroxide formation and chronopotentiometric measurement were recorded across the resistor of 6 MΩ under flow and stagnant conditions. The transition of fluorescence signal from a to b implies the higher production of hydrogen peroxide whereas the transition from b to c implies the removal of hydrogen peroxide from the GDL and the arrival of the fresh reactant under continuous flow conditions.

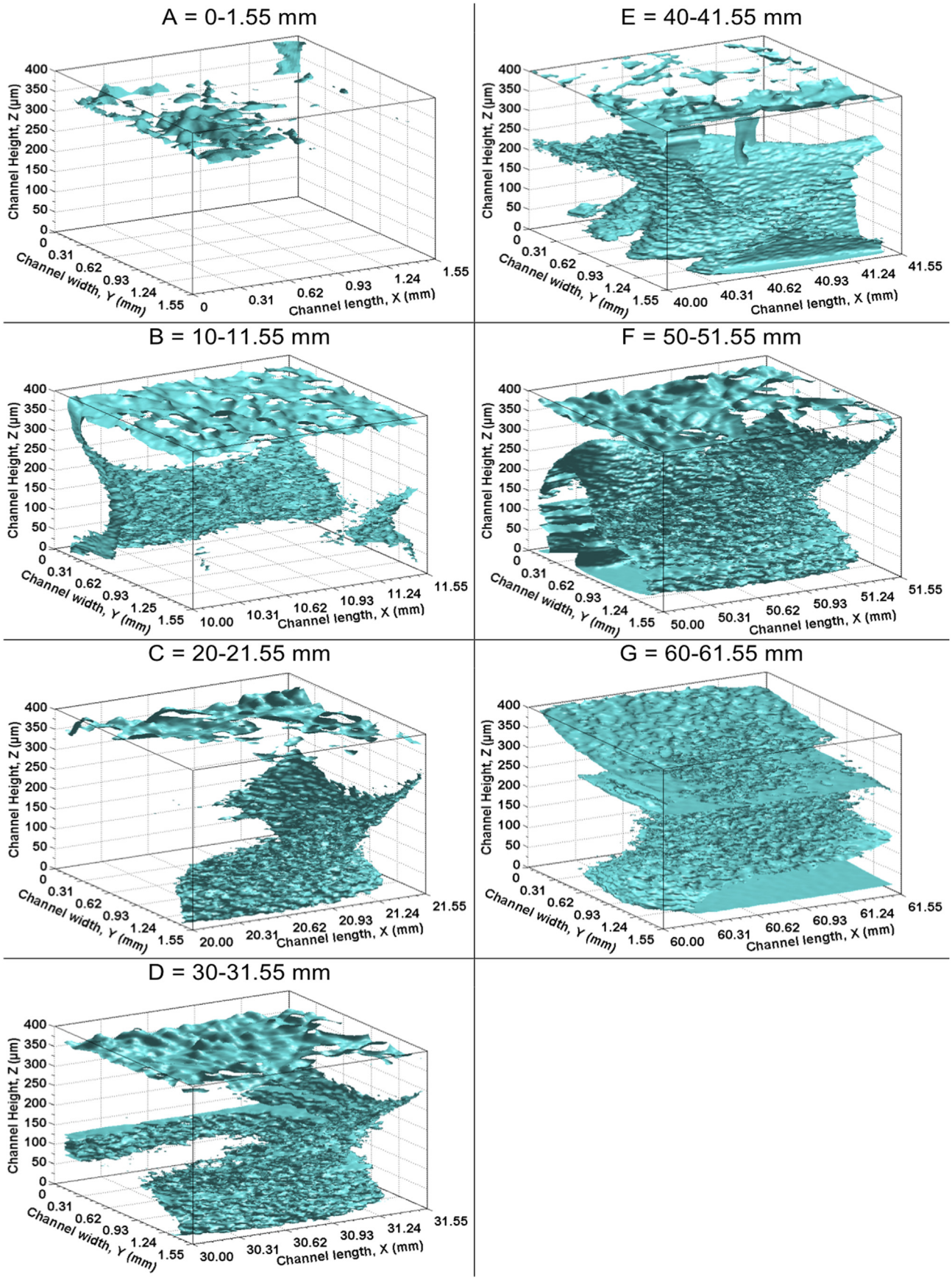

Fig. 9. Three-dimensional isosurface plots of hydrogen peroxide distribution in the cathodic chamber, produced at the operating potential of 300 mV. The seven view positions are assigned as A to G according to the channel geometry in Fig. 12. The blue colour represents the presence of hydrogen peroxide. (For interpretation of the references to colour in this figure legend, the reader is referred to the web version of this article.)

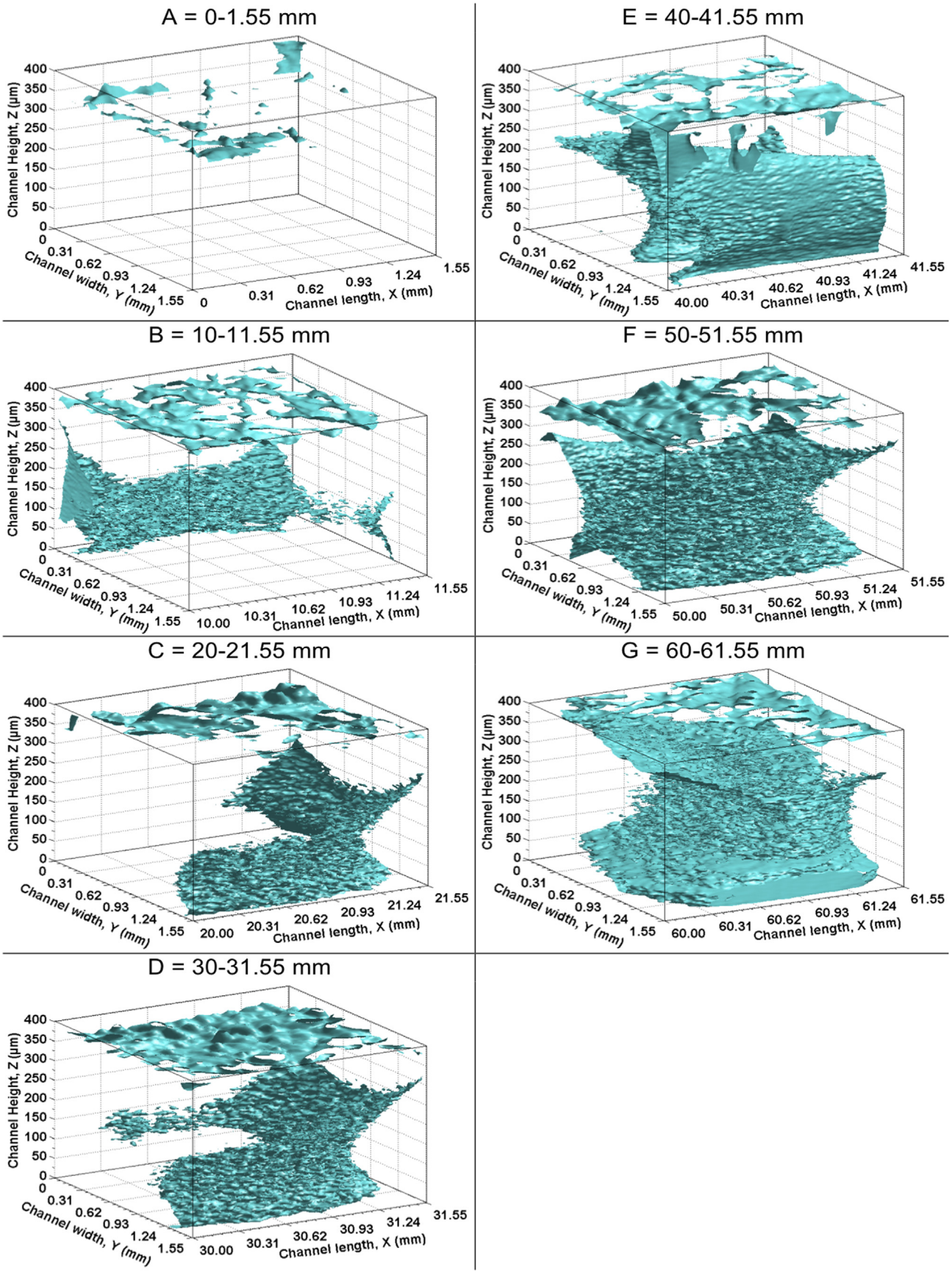

Fig. 10. Three-dimensional isosurface plots of hydrogen peroxide distribution in the cathodic chamber, produced at the operating potential of 400 mV. The seven view positions are assigned as A to G according to the channel geometry in Fig. 12. The blue colour represents the presence of hydrogen peroxide. (For interpretation of the references to colour in this figure legend, the reader is referred to the web version of this article.)

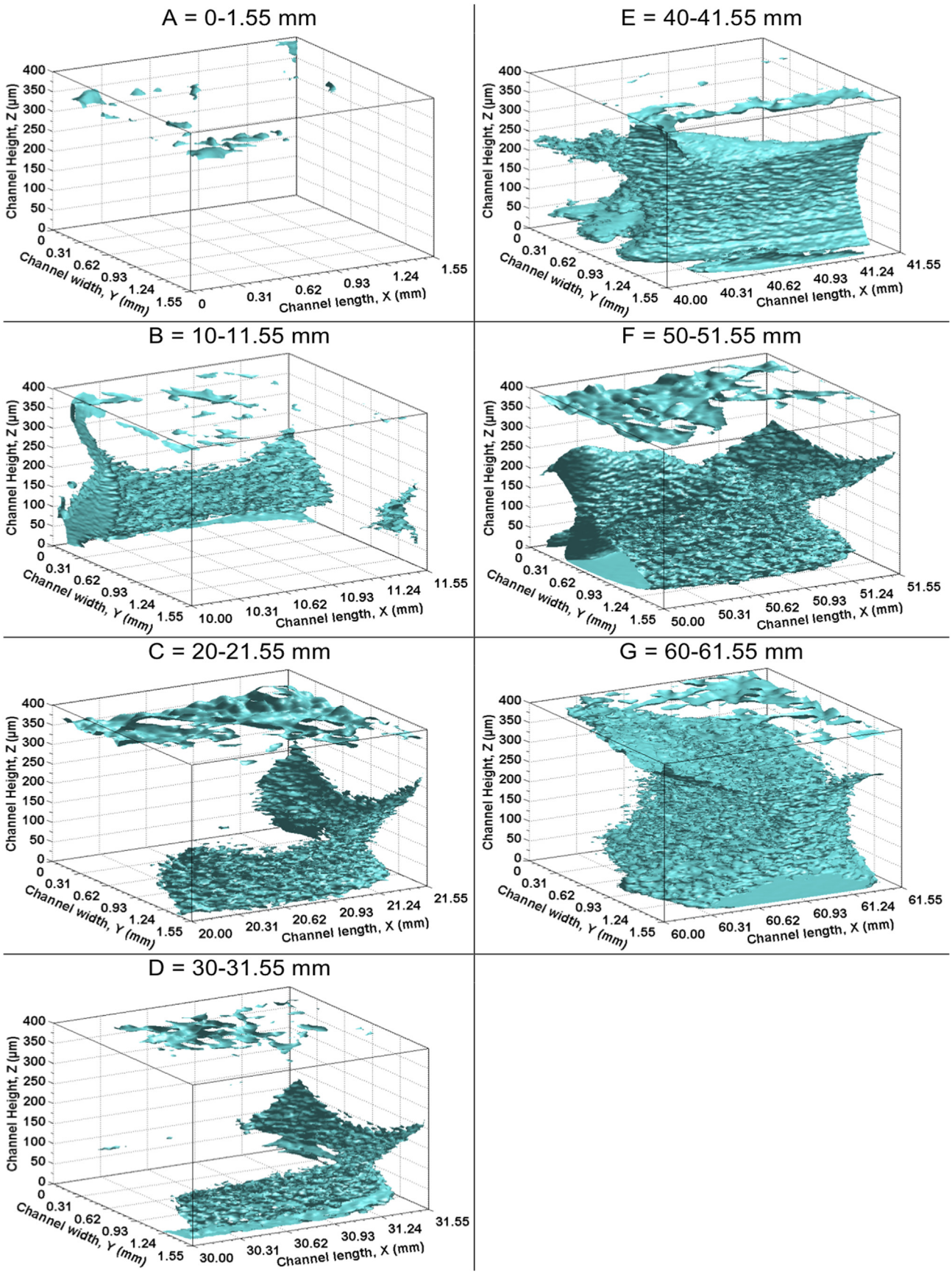

Fig. 11. Three-dimensional isosurface plots of hydrogen peroxide distribution in the cathodic chamber, produced at the operating potential of 550 mV. The seven view positions are assigned as A to G according to the channel geometry in Fig. 12. The blue colour represents the presence of hydrogen peroxide. (For interpretation of the references to colour in this figure legend, the reader is referred to the web version of this article.)

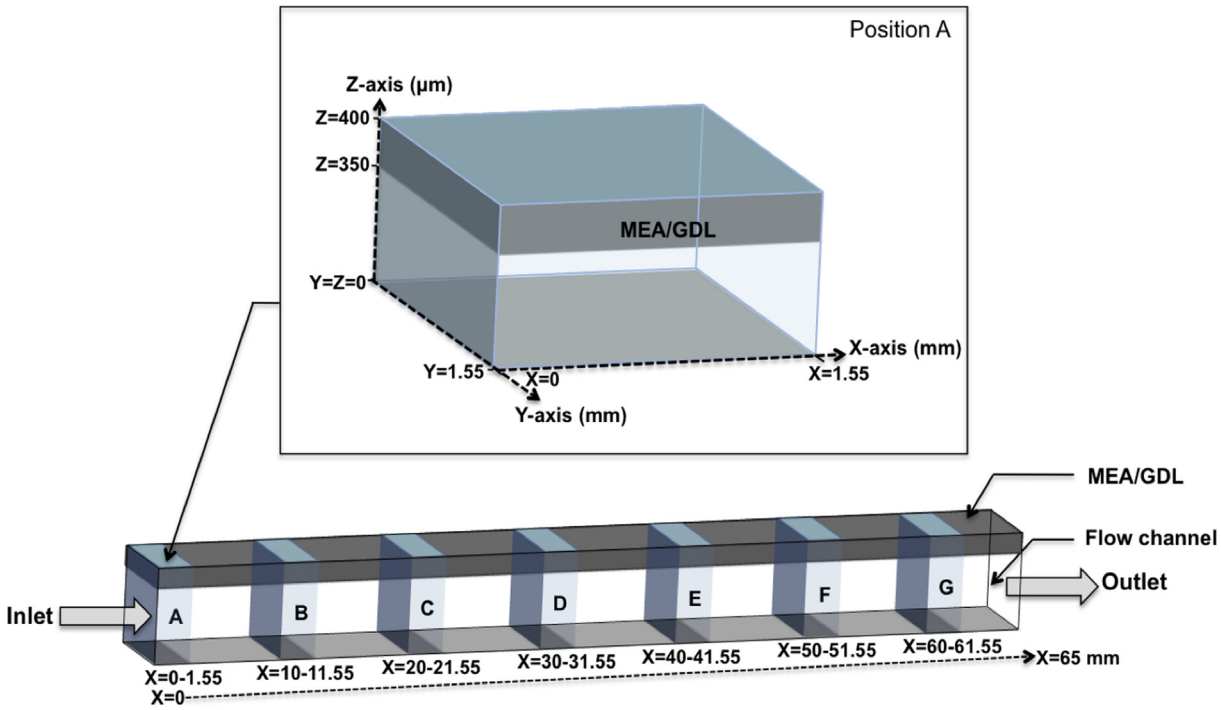

Fig. 12. The geometry of the cathodic chamber for simultaneous investigations. The cathodic chamber is composed of the flow channel and the GDL. Seven positions along channel length (*X*-axis) were investigated and assigned as A to G, where $X = 0$ is the inlet and $X = 65$ mm is the outlet. In the *Z*-axis, the *Z* position of 0–350 μm refers to the positions in the flow channel whereas the *Z* position of 350–400 μm refers to the position from the GDL's surface to 50 μm inside the GDL. Each view section has a dimension of 1.55 mm wide × 1.55 mm long × 400 μm high.

by confocal microscopy. It is noted that the equation is valid when the average fluorescence intensity is in the range of 35–165.

3.3. Visualisation and quantification of hydrogen peroxide formation

The hydrogen peroxide formation was investigated within the GDL, along with the potential response of the DMFC. The time-series visualisation of hydrogen peroxide formation within the GDL is illustrated in Fig. 7. The confocal images demonstrate the view of GDL and hydrogen peroxide formation taken inside the GDL (at 50 μm away from the GDL's surface toward the PEM). The green colour represents the reflection of the carbon spindles in the GDL whereas the red colour represents a fluorescent signal. The corresponding three-dimensional plot of fluorescence intensity is also displayed next to each confocal image to improve the visibility of hydrogen peroxide formation and transport. Both confocal images and three-dimensional intensity plots reveal an increase in fluorescent intensity over time, indicating the formation of hydrogen peroxide inside the GDL. The dark spot located near the GDL centre throughout the examination period is caused by the incomplete wetting of teflonated GDL.

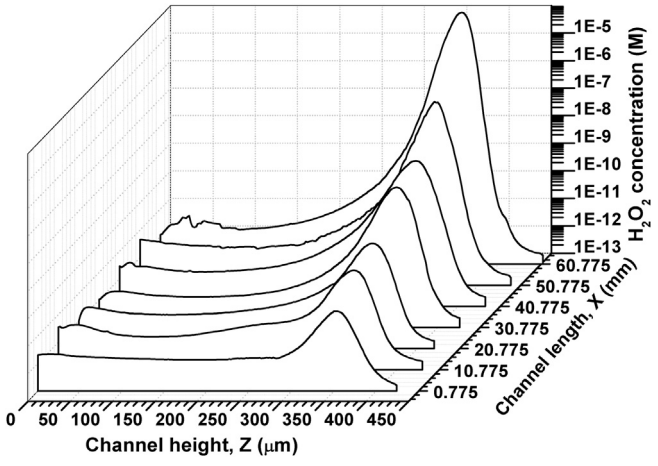

Fig. 13. Average concentration of hydrogen peroxide produced at the operating potential of 300 mV, determined by the fluorescence mapping. The channel length (*X*) and height (*Z*) are assigned according to the channel geometry in Fig. 12.

A correlation between the average fluorescence intensity and the potential response is shown in Fig. 8. The change in the fluorescence intensity is attributed to the production/removal of hydrogen peroxide at this focal plane. Under flow conditions, the average fluorescence intensity gradually increases with a pulse signal sequence (every 550 s) throughout the investigation. The increasing fluorescence signal for each pulsing peak (e.g. the transition from a to b in Fig. 8) implies the higher production of hydrogen peroxide while the pulsing phenomena are probably caused by two different factors: (i) the use of pulsating pump and (ii) the removal of hydrogen peroxide from the GDL and the arrival of the fresh reactant under continuous flow conditions (as shown in the transition from b to c).

The correlation can be simply explained in chronological order according to Fig. 8. From $t = 0$ to $t = 3500$ s, the average fluorescence intensity rapidly increases while the cell potential quickly drops as a function of time. The higher production of hydrogen peroxide promotes the fluorescence signal but reduces the cell potential. When the reaction continues further from $t = 3500$–5000 s, the cell potential slightly reduces. The fluorescence intensity continues increasing due to the greater production of hydrogen peroxide within the GDL.

It can be concluded that there is a correlation between the production/accumulation of hydrogen peroxide and the cell

potential. In order to maintain the cell performance, hydrogen peroxide should be efficiently removed from the fuel cell. Therefore, it is important to understand how hydrogen peroxide transports and accumulates in the cathodic chamber. The study is described in the following section.

3.4. Three-dimensional distribution and production of hydrogen peroxide and current efficiency at different operating potential

The distribution of hydrogen peroxide generated from the electrocogeneration process was investigated at various cell potentials, which is illustrated in Figs. 9–11. The blue colour represents the presence of hydrogen peroxide in the cathodic chamber. The isosurfaces are plotted corresponding to the channel geometry in Fig. 12. The three-dimensional visualisation, composed of single XY images taken along the channel height (Z-axis) with an interval of 1 μm, was carried out at seven positions along the channel length (X-axis = 0–65 mm). Each view section has a dimension of 1.55 mm wide × 1.55 mm long × 400 μm high. In the Z-axis, the Z position of 0–350 μm refers to the positions in the flow channel whereas the Z position of 350–400 μm refers to the position from the GDL's surface to 50 μm inside the GDL.

It is found that hydrogen peroxide is densely packed inside the GDL. This indicates that once hydrogen peroxide was produced at the three-phase zones, a certain amount of hydrogen peroxide was trapped inside the GDL. As hydrogen peroxide is also detected around the edge and wall of the flow channel, it implies that some of hydrogen peroxide broke through the GDL and subsequently mixed with the fresh reactant in the flow channel. Despite under flow conditions, hydrogen peroxide could be partially removed by the forced convection according to the velocity profile of laminar flow ($Re < 2000$). Basically, the velocity distribution at a cross section is parabolic in shape where the velocity of the fluid in contact with the channel wall is close to zero and increases further away from the wall to the maximum velocity at the centre [16]. After the middle length of the channel (i.e. $X = 30$–31.55 mm), hydrogen peroxide gradually disperses and then spreads through the entire channel near the outlet ($X = 60$–61.55 mm). Considering that the volume flow rates at the inlet and the outlet were the same, the production of hydrogen peroxide increased along the channel length.

The influence of the operating potential on the production of hydrogen peroxide can be evaluated by comparison among Figs. 9–11. Amount of hydrogen peroxide production is much higher with decreasing the cell potential. Accordingly, the operating potential of 300 mV enables the extensive detection of hydrogen peroxide in comparison with the higher potentials of 400 and 550 mV. Next, the concentration of hydrogen peroxide produced at various cell potentials was quantified using fluorescence mapping according to the fitted Equation (6) as shown in Figs. 13–15. The concentration of hydrogen peroxide production is plotted over the channel position X and Z as schematically described in Fig. 12. In comparison among the cell potentials, the maximum hydrogen peroxide concentrations of 137.62, 23.67 and 5.44 μM were generated at the operating potentials of 300, 400 and 550 respectively. For all cell potentials, the maximum concentration of hydrogen peroxide was located near the GDL's surface (i.e. $Z \sim 350$ μm), in which hydrogen peroxide shortly broke through the GDL. After that, hydrogen peroxide mixed with the fresh reactants in the flow channel ($Z < 350$ μm) that led to a depletion of hydrogen peroxide detection. On the other hand, a dramatic decrease in the fluorescence signal inside the GDL ($Z > 350$ μm) was caused by the loss of instrumental sensitivity in an opaque specimen.

In addition to the quantification of hydrogen peroxide production using confocal microscopy, the current density generated from various cell potentials was also monitored concurrently as

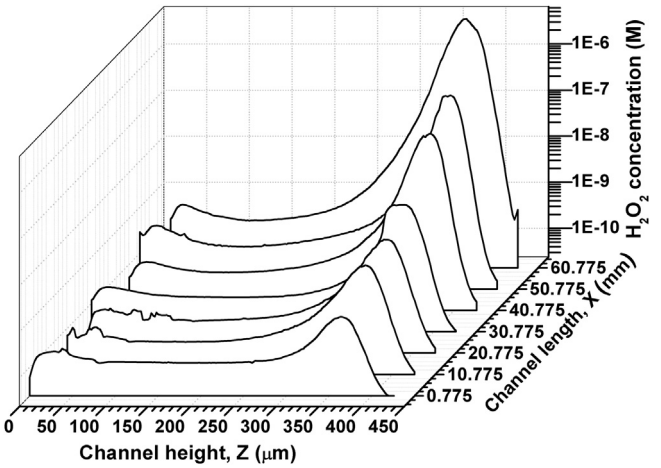

Fig. 14. Average concentration of hydrogen peroxide produced at the operating potential of 400 mV, determined by the fluorescence mapping. The channel length (X) and height (Z) are assigned according to the channel geometry in Fig. 12.

illustrated in Fig. 16. The inset in Fig. 16 demonstrates that the current densities of 2360, 1128 and 114 μA $cm^{-2}$are initially generated from the cell potentials of 300, 400 and 550 mV respectively. After that, the current densities drop to 248.08, 86.54 and 33.15 μA cm^{-2}, respectively, within 60 s. The current densities were highly produced at the beginning of the operation because the dissolved oxygen was greatly available at the three-phase zones. When the reaction occurred for a longer period of time, the diminution of electrocatalytic activity at both electrodes caused the reduction of current density. Specifically, the catalyst poisoning could occur as a consequence of the incomplete oxidation of methanol which then forms carbon monoxide as an adsorbed layer at the platinum catalyst. Another possible reason for that is the inefficient removal of by-products which minimises the active surface area for the half–cell reactions to occur.

The effect of the cell potential on current efficiency was evaluated by the simultaneous investigations. The current efficiency is a ratio between the experimental and theoretical amount of hydrogen peroxide production. In this work, the experimental amount of hydrogen peroxide production was determined by the interpolation of the data obtained by means of confocal microscopy (as shown in Figs. 13–15). The theoretical amount of hydrogen

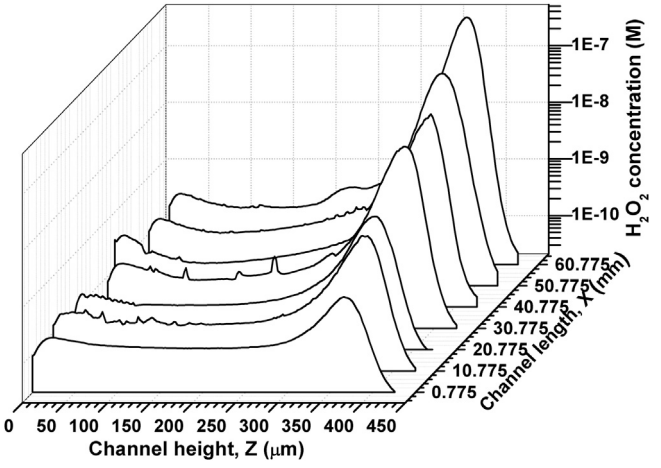

Fig. 15. Average concentration of hydrogen peroxide produced at the operating potential of 550 mV, determined by the fluorescence mapping. The channel length (X) and height (Z) are assigned according to the channel geometry in Fig. 12.

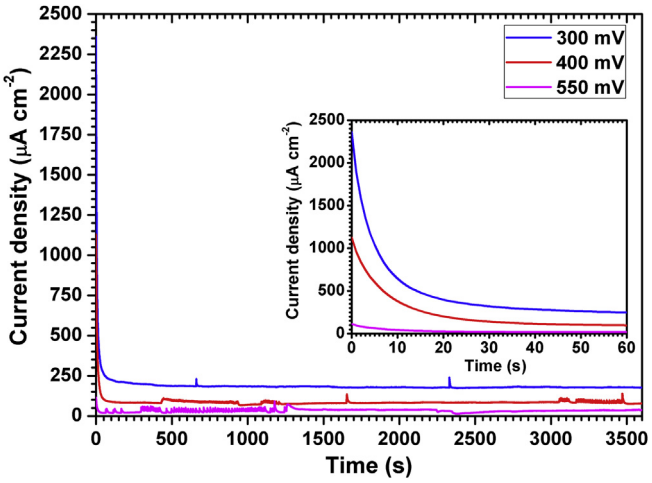

Fig. 16. Current density simultaneously recorded during the visualisation shown in Figs. 13–15, at cell potentials of 300, 400 and 550 mV. The inset highlights the dramatic decrease in the current density on an enlarged timescale.

peroxide production was calculated from the total charge generated which was a function of the current response at a given period of time (Fig. 16). The current efficiencies of 85.00, 64.78 and 51.13% were obtained from the DMFC operating at the cell potentials of 300, 400 and 550 mV respectively.

It can be concluded that the cogeneration of current density and hydrogen peroxide was improved when the cell potential was reduced from 550 to 300 mV. In other words, decreasing of cell potential can drive more reactions towards the favourable two-electron transfer reduction. For an ideal cogeneration system, this system should undergo absolute two-electron transfer reduction to provide a useful amount of electricity and hydrogen peroxide. These fundamental studies have answered some of the critical challenges and have also established an alternative analytical tool, which are beneficial to the development of a practical electro-cogeneration system.

4. Conclusions

The DMFC with an electrocogeneration system developed in this work can generate current density of 4.5–5.3 mA cm^{-2} and power density of 0.8–1.2 mW cm^{-2}. Despite relatively low performance, the visualisation of hydrogen peroxide production and removal in the cathodic chamber can be achieved using confocal microscopy. It is a promising tool to verify the existence of hydrogen peroxide and to monitor the electrocogeneration process while simultaneously measuring the potential response and the current generated. As the fluorescence signal is influenced by the amount of hydrogen peroxide generated, a correlation between the production/accumulation of hydrogen peroxide and the cell potential can be obtained; the higher production of hydrogen peroxide promotes the fluorescence signal but reduces the cell potential due to the depletion of fresh reactant and the accumulation of hydrogen peroxide at the active sites. With the application of forced convection to the flow channel, the efficiency of hydrogen peroxide removal is greatly improved to certain extent according to the velocity profile under laminar flow; hence, the accumulation of hydrogen peroxide is located near the channel wall. Considering that the volumetric flow rates at the inlet and the outlet are identical, the distribution of hydrogen peroxide toward the center part within the flow channel increases progressively along the channel length indicating that the larger amount of hydrogen peroxide is generated. Furthermore, the cogeneration of current density and hydrogen peroxide is significantly improved when the cell potential is reduced. Specifically, the maximum hydrogen peroxide concentrations of 137.62, 23.67 and 5.44 μM and the current efficiencies of 85.00, 64.78 and 51.13% are obtained at the operating potentials of 300, 400 and 550 mV respectively.

Acknowledgements

The authors gratefully acknowledge the financial support of National Metal and Materials Technology Center (P1200990), Royal Thai Government and Faculty for the Future (Schlumberger). The authors are grateful to Dr. Rob Potter and Dr. Andrew York from Johnson Matthey Technology Centre, Reading-UK, for the supply of electrode materials used in this research and also for their useful suggestions, advice and technical expertise throughout the experimental work.

References

[1] F. Alcaide, P.-L. Cabot, E. Brillas, J. Power Sources 153 (2006) 47–60.
[2] S. Srinivasan, Fuel Cells: From Fundamentals to Applications, first ed., Springer, New York, 2006.
[3] L. Stanley, F. Iraj, Q. Colin, J. Am. Chem. Soc. 97 (1975) 4786–4787.
[4] X.-Z. Yuan, Z.-F. Ma, Q.-G. He, J. Hagen, J. Drillet, V.M. Schmidt, Electrochem. Commun. 5 (2003) 189–193.
[5] E. Brillas, F. Alcaide, P.-L. Cabot, Electrochim. Acta 48 (2002) 331–340.
[6] F. Alcaide, E. Brillas, P.-L. Carbot, J. Casado, J. Electrochem. Soc. 145 (1998) 3444–3449.
[7] I. Yamanaka, T. Onizawa, S. Takenaka, K. Otsuka, Angew. Chem. Int. Ed. 42 (2003) 3653–3655.
[8] G. Strukul, Catalytic Oxidations with Hydrogen Peroxide as Oxidant, first ed., Kluwer Academic Publishers, USA, 1992.
[9] C. Oloman, A.P. Watkinson, J. Appl. Electrochem 9 (1979) 117–123.
[10] K. Otsuka, I. Yamanaka, Electrochim. Acta 35 (1990) 319–322.
[11] G. Agladze, P. Nikoleishvili, G. Tsurtsumia, V. Kveselava, G. Gorelishvili, R. Latsuzbaia, J. Electrochem. Soc. 157 (2010) 140–147.
[12] R. Cathcart, E. Schwiers, B.N. Ames, Anal. Biochem. 134 (1983) 111–116.
[13] C.N. Murray, J.P. Riley, Deep Sea Res. Oceanogr. Abstr. 16 (1969) 311–320.
[14] X. Ren, T.E. Springer, T.A. Zawodzinski, S. Gottesfeld, J. Electrochem. Soc. 147 (2000) 466–474.
[15] S.K. Kamarudin, W.R.W. Daud, S.L. Ho, U.A. Hasran, J. Power Sources 163 (2007) 743–754.
[16] S.L. Post, Applied and Computational Fluid Mechanics, first ed., Jones & Bartlett Publishers, USA, 2009.